Regime switching on the propagation speed of travelling waves of some size-structured Myxobacteria population models

Vincent Calvez, Adil El Abdouni, Maxime Estavoyer, Ignacio Madrid, Julien Olivier, Magali Tournus

Regime switching on the propagation speed of travelling waves of some size-structured Myxobacteria population models*

Vincent Calvez[1], Adil El Abdouni[2], Maxime Estavoyer[3], Ignacio Madrid[4], Julien Olivier[5], Magali Tournus[5].

[1]Univ Lyon, CNRS, Université Claude Bernard Lyon 1, UMR5208,
Institut Camille Jordan, F-69622 Villeurbanne, France
[2]Laboratoire de Mathématiques de Versailles, UVSQ, CNRS, Université Paris-Saclay
45 Avenue des États-Unis, 78035 Versailles cedex
[3] Inria, and Université de Lyon, Université Claude Bernard Lyon 1,
CNRS UMR 5208, Institut Camille Jordan, Villeurbanne Cedex, France
[4] CMAP, CNRS, École polytechnique, Institut Polytechnique de Paris,
91120 Palaiseau, France
[5] Aix Marseille Univ, CNRS, Centrale Marseille, I2M, UMR 7373,
Turing Centre for Living systems, Marseille, France

*This project has received funding from the European Research Council (ERC) under the European Union's Horizon 2020 research and innovation programme (grant agreement No 865711).

Abstract

The spatial propagation of complex populations can depend on some structuring variables. In particular, recent developments in microscopy have revealed the impact of bacteria heterogeneity on the population motility. Biofilms of *Myxococcus xanthus* bacteria have been shown to be structured in clusters of various sizes, which remarkably, tend to move faster when they consist of a larger number of bacteria. We propose a minimal reaction-diffusion discrete-size structure model of a population of *Myxococcus* with two possible cluster sizes: isolated and paired bacteria. Numerical experiments show that this model exhibits travelling waves whose propagation speed depends on the increased motility of clusters, and the exchange rates between isolated bacteria and clusters. Notably, we present evidence of the existence of a characteristic threshold level θ^* on the ratio between cluster motility and isolated bacteria motility, which separates two distinct regimes of propagation speed. When the ratio is less or equal than θ^*, the propagation speed of the population is constant with respect to the ratio. However, when the ratio is above θ^*, the propagation speed increases. We also consider a generalised model with continuous-size structure, which also shows the same behaviour. We extend the model to include interactions with a resource population, which show qualitative behaviours in agreement to the biological experiments.

1 Introduction

Recent developments in high-throughput cell segmentation techniques have allowed microbiologists to closely follow complexly structured bacterial populations [1]. Interactions between individuals, both cooperative and competitive, and the emergence of subpopulations with distinct behaviours, have revealed the effects that this underlying structure might have across the different scales of the population dynamics [2, 3]. One important aspect that might be affected is the way they explore their surroundings.

One interesting example of this is the behaviour of *Myxococcus xanthus*, a species of motile predatory bacteria found in soil which forms multicellular biofilms to prey on other microorganisms [4]. Thanks to high-throughput microscopy techniques, it has been shown that this biofilm has not a homogeneous structure, but is in fact composed of bacteria clusters of various sizes, from isolated individuals, to large swarms of closely packed bacteria. In particular, recent works have shown that these clusters can exhibit distinct motility behaviours, which depend on their size and composition. This affects the macroscopic motility of the biofilm during the predatory incursions [5].

In particular, the cluster structure of *M. xanthus* populations has been shown to be determined by the phenotypic heterogeneity among individual cells [5]. Indeed, *M. xanthus* cells are capable to switch between two different motility regimes, namely: the adventurous A-motility, and the social S-motility, which result from the expression of two distinct sets of genes [6]. A-motile cells can glide over the surface, using a complex protein machinery that anchors and pushes the cell forward. S-type motion, on the other hand, is contact-dependent. S-motile cells move thanks to the projection of pili, hair-like structures that grow from the cell and can attach to other cells or the surrounding extracellular matrix, to then retract and drag the cell. This movement depends on the presence of a key component of the extracellular matrix: the exopolysaccharides (EPS). EPS is secreted and left as a chemical trail by *M. xanthus* as it moves, which allows the adhesion and cohesion of cells, thus favouring the emergence of swarms of bacteria which move collectively.

Importantly, the proportion of A-motile and S-motile cells, and therefore, the distribu-

tion of the cluster sizes, has been shown to impact the fitness of *M. xanthus* populations. On the one hand, predation is initiated by pioneer A-motile cells that explore the area around the colony first. On the other hand, the collective motion of S-motile cells can increase the efficiency of predation, since killing is contact-dependent [7]. Therefore, both motility systems play synergistic roles [5].

In this work, we aim to study the impact of cellular cohesion on the global motility of the population. In particular, we will focus on population dynamics in which individuals have an advantage when coagulating (social synergy), which is expressed as a higher motility. To that extent, we will consider some structured population models, with a spatial position variable and a structuring variable which corresponds to the cluster size. Clusters of different sizes may grow, divide, and coagulate, and based on previous observations, larger clusters will diffuse at higher rates [8].

The paper is organised as follows. In Section 2 we present the various models that we will study. First, we present a "discrete" model in which we only consider two cluster sizes: singletons of isolated A-motile bacteria, and clusters of two S-motile bacteria. Next, we present a continuous cluster-size model that generalises this model, accounting for the possibility to produce, through fragmentation and coagulation, clusters of any size. Finally we consider a derived predator-prey model, where the bi-type clustered population introduced in the first model will interact with a prey population of *E. coli*. In Section 3, we study theoretically and numerically the discrete model. In Section 4 and Section 5, we do the same for respectively the continuous model and the predator-prey model.

2 Proposed models and main results

2.1 Discrete size model

Let us consider first a minimal model in which we have isolated bacteria (i.e. clusters of size one) and paired bacteria (clusters of size two) that move in the real line. We suppose that both species are well mixed and call $p_1(x,t)$ the density of isolated bacteria, and $p_2(x,t)$ the density of clusters of size two, at a given location in space $x \in \mathbb{R}$ and at a given time $t \geq 0$. We suppose that p_1 and p_2 solve the following system of two

reaction–diffusion partial differential equations:

$$\partial_t p_1 = \theta_1 \Delta p_1 - \tau_1 p_1^2 + 2\tau_2 p_2 + \alpha p_1 \left(1 - \frac{p}{K}\right), \tag{1}$$

$$\partial_t p_2 = \theta_2 \Delta p_2 + \frac{\tau_1}{2} p_1^2 - \tau_2 p_2, \tag{2}$$

with p the total number of bacteria, $p = p_1 + 2p_2$.

The first terms in the right-hand side of Equations (1) and (2) are diffusion terms, and describes respectively the spatial random movement of isolated bacteria and clusters of bacteria. We assume that $\theta_2 > \theta_1$, *i.e.* clusters spread faster than isolated bacteria. The second term $\tau_1 p_1^2$ represents the coagulation of isolated bacteria, which happens at rate $\tau_1 > 0$ and changes two isolated bacteria into one cluster of size two. The term $\tau_2 p_2$ corresponds to the fragmentation of clusters of size two, which happens at rate $\tau_2 > 0$ and produces two isolated bacteria. Moreover, we assume that only isolated bacteria can divide. This growth term is assumed to be logistic, with growth rate $\alpha > 0$ and carrying capacity of the environment K. The model (1)-(2) is an extension of the Fisher-KPP model [9, 10], which reduces to the Fisher-KPP equation when $\tau_1 = \tau_2 = 0$ and $p_2(t = 0, \cdot) = 0$. In that case, the propagation minimal speed is well known to be given by $c^* = 2\sqrt{\alpha\theta_1}$.

Numerical simulations of this system, presented in Section 3, suggest the existence of travelling waves solutions for all positive parameters. Moreover, we observe two distinct regimes separated by a constant threshold level θ^* for the ratio θ_2/θ_1. When $\theta_2/\theta_1 < \theta^*$, the critical speed of the travelling wave of p is equal to the critical speed $c^* = 2\sqrt{\alpha\theta_1}$ of the equation (1) without coagulation and fragmentation. When $\theta_2/\theta_1 > \theta^*$, the critical speed of the travelling wave becomes strictly larger than this value. There are two possible explanations for this phenomenon: the existence of an anomalous speed [11] and the nonlinear interaction of the coagulation term. For the first phenomenon, the increase in speed is caused by the linear terms of the system, and mainly by the coupling induced by the fragmentation term. In the second case, the increase is explained by the presence of the nonlinear coagulation term, in which case the propagation front being referred to as *pushed* waves. Conversely, when the front is determined linearly, the front is called a *pulled* front. A formal definition of pulled and pushed waves in the context of the *inside dynamics* of

the population can be consulted in [12]. In a subsequent work not reported in this article [13], we show that, for $\theta_2/\theta_1 > \theta^\star$, the numerical speed of the traveling wave does not correspond to the anomalous linear speed. Therefore, in this article we numerically study the transition between pulled and pushed fronts. In biological terms, we conclude that when the motility of clusters is significant enough with respect to the motility of isolated bacteria, the collective behaviour of *M. xanthus* allows the whole population to propagate faster than in the asocial case. We also study the system theoretically and numerically under the assumptions $\tau_1, \tau_2 \to +\infty$. In this case, the system reduces to a scalar equation.

2.2 Continuous cluster-size model

Empirically, the cluster structure of *M. xanthus* swarms can vary from lonely scout cells to thousands of densely packed social bacteria. We can extend the model (1)-(2) to a general Diffusion-Growth-Fragmentation-Coagulation model, described by (3)-(6), where we define $\rho(t, x, z)$ as the density at position $x \in \mathbb{R}$ and time $t \geq 0$ of clusters of size $z \in [0, z_{max}]$ (or more precisely, the total mass or volume of the cluster, which is a continuous variable), with $z_{\max} \in \mathbb{R}_\star^+ \cup \{+\infty\}$ the maximum admissible size. The model is defined by the following integro-differential equation:

$$\partial_t \rho(t,x,z) = \partial_{xx}\left[\theta(z)\rho(t,x,z)\right] - \partial_z\left[v(z, m(t,x))\rho(t,x,z)\right] + \mathcal{F}[\rho](t,x,z) + \mathcal{G}[\rho](t,x,z), \quad (3)$$

with

$$\mathcal{F}[\rho](t,x,z) = 2\int_z^{z_{\max}} \beta(z')k(z',z)\rho(t,x,z')\ dz' - \beta(z)\rho(t,x,z), \quad (4)$$

$$\mathcal{G}[\rho](t,x,z) = \frac{1}{2}\int_0^z \gamma(z-z',z')\rho(t,x,z-z')\rho(t,x,z')\ dz' - \rho(t,x,z)\int_0^{z_{\max}-z} \gamma(z',z)\rho(t,x,z')dz', \quad (5)$$

and

$$m(t,x) = \int_0^{z_{\max}} z'\rho(t,x,z')\ dz'. \quad (6)$$

As before, the first term in (3) corresponds to the spatial diffusion of the clusters. The diffusion coefficient of a cluster is a function of its size. The second term in (3) is a transport term representing the growth of cluster size through cell division within each cluster. The function $v(z, m) \geq 0$ is the instantaneous growth speed of a cluster of size z when the total mass at its spatial position is m, as defined by (6). In $z = 0$, we assume this speed to be zero, hence no condition is required at this boundary. Notice that the division mechanism conveyed by this term is different than the one considered in (1)-(2), conveyed by a proliferation term. Indeed, we made the simplifying assumption that a dividing bacterium will necessarily increase the size of its cluster. We assume that this speed is zero for clusters of maximal size, $z_{\max}$. The third term in (3), defined in (4), corresponds to the fragmentation of clusters, which occurs at a fragmentation rate $\beta(z) \geq 0$, which is a function of the cluster size. When a cluster of size z' fragments, it produces two clusters of respective sizes z and $z' - z$ with probability $k(z', z)dz = k(z', z' - z)dz$. The first term in (4) corresponds to the creation of clusters of size z by the fragmentation of a cluster of larger size, while the second term corresponds to the loss of clusters of size z due to fragmentation into clusters of smaller sizes. Finally, the last term in (3) corresponds to the coagulation of clusters, as defined by the operator in (5). Two clusters of respective sizes z and z' coagulate at a rate $\gamma(z, z')$, which we call the coagulation rate. We assume that the coagulation rate is symmetrical, $\gamma(z, z') = \gamma(z', z)$. The first term in (5) corresponds to the creation of clusters of size z through the coagulation of clusters of sizes z' and $z - z'$, with $z' < z$. The second term corresponds to the loss of clusters of size z through coagulation with clusters of any other size.

The existence of travelling waves in spatial models with continuous structure has been studied by various authors in many particular cases (for example [14, 15, 16, 17]). However, to our knowledge, the existence of travelling waves in structured populations involving a coagulation operator is being studied numerically for the first time in this work. For the presented numerical simulations, we select specific functions for the fragmentation, division, and coagulation rates. For these specific choices, we exhibit numerically the existence of travelling waves connecting the null function to the stationary solution of the problem without spatial diffusion. As for the discrete model, we notice the existence of

a diffusion coefficient value corresponding to a threshold. That is, for a smaller diffusion coefficient, the wave speed is constant with respect to this parameter and for a larger value, the wave speed increases.

2.3 Predator-resource model

M. xanthus are predator bacteria. This predation is initiated by isolated cells known as *scouts*, which explore the surroundings of the colony to identify potential nutrient sources [18]. Their attack strategy depends on several parameters, but it depends crucially on the prey density [19]. This way, as prey become scarce, *M. xanthus* increase their scouting capabilities. Once the prey has been found, they can switch behaviours to start killing the prey and consuming the nutriments released by the prey. Although the exact mechanism used by *M. xanthus* to kill its prey is not fully understood, it is known that cell killing can only occur in close proximity to *M. xanthus* (contact-dependent) [20, 21]. Moreover, cluster size structure also play an important role in predation. While the forefront of the assault is mainly constituted by singletons or small groups of scouts, the rear of the front consists of rather large clusters exhibiting distinct macroscopic behaviours, called *swarms* [5].

To model this phenomenon, we propose a new model in which we assume the existence of two additional bacterial types: diffusive individuals, which move around alone or in clusters, and eating individuals, consisting of isolated bacteria and clusters capable to kill and consume the prey, but remaining immobile. This supplementary structure gives a total of four subtypes. For this model, we consider a two-dimensional space. We denote by $\rho_1^D(x,y,t)$ the density of isolated bacteria in the diffusing state, and $\rho_1^E(x,y,t)$ the density of isolated bacteria in the eating state, which are solutions to the following equations

$$\partial_t\, \rho_1^D = \theta_1 \Delta \rho_1^D + \alpha_D \rho_1^D (1-\rho) - \tau_1^{DE}(e)\rho_1^D + \tau_1^{ED}(e)\rho_1^E - \tau_1(\rho_1^D)^2 + 2\tau_2\rho_2^D, \qquad (7)$$

$$\partial_t\, \rho_1^E = \alpha_E(\rho_1^E + 2\rho_2^E)(1-\rho) + \tau_1^{DE}(e)\rho_1^D - \tau_1^{ED}(e)\rho_1^E - \tau_1(\rho_1^E)^2 + 2\tau_2\rho_2^E. \qquad (8)$$

On the other hand, the density of clusters of two bacteria in diffusing state, $\rho_2^D(x,y,t)$,

and those which eat, $\rho_2^E(x,y,t)$, are given by

$$\partial_t\ \rho_2^D = \theta_2 \Delta \rho_2^D + \frac{\tau_1}{2}(\rho_1^D)^2 - \tau_2 \rho_2^D - \tau_2^{DE}(e)\rho_2^D + \tau_2^{ED}(e)\rho_2^E, \tag{9}$$

$$\partial_t\ \rho_2^E = \tau_2^{DE}(e)\rho_2^D - \tau_2^{ED}(e)\rho_2^E + \frac{\tau_1}{2}(\rho_1^E)^2 - \tau_2 \rho_2^E. \tag{10}$$

As previously we are interested in the situation in which clusters have got an enhanced motility, so $\theta_2 > \theta_1$. Finally, the density of the prey, which is supposed to be immobile, is given by

$$\partial_t\ e = -\delta_1 \rho_1^E - \delta_2 \rho_2^E, \tag{11}$$

with δ_1 and δ_2 being the consumption rates of the prey by, respectively, isolated predatory bacteria in the "eating" state and clusters of predatory bacteria in the "eating" state. In our model, the prey bacteria corresponds solely to a resource. We do not focus on its own dynamics but on its interaction with the predatory bacteria. We assume that the dispersion of the prey is negligible.

In equations (7) and (8) we define ρ as the total of predatory bacteria, *i.e.* $\rho = \rho_1^E + \rho_1^D + 2\rho_2^E + 2\rho_2^D$. The model (7)-(11) is schematized in figure 1. We assume that the change between the "diffusion" state and the "eating" state is dependent on the local amount of prey. Diffusing bacteria can change state with a certain rate τ_i^{DE}, and conversely bacteria become diffusing with a rate τ_i^{ED}, with $i = 1$ or $i = 2$ which corresponds to the size of the cluster. For this model, we assume that a bacteria in a cluster of two bacteria consuming the prey can divide to produce an isolated bacteria. We assume that bacteria that consume have a significant division advantage compared to isolated bacteria that disperse ($\alpha_E > \alpha_D$). The transitions between the clusters of two bacteria and the isolated bacteria are the same as in the previous model. The proliferation terms are assumed to be logistic with a carrying capacity dependent on the total number of bacteria, ρ. For the model (7)-(11), the Laplacian operator only depends on space, *i.e.*, $\Delta u(x,y,t) = \partial_{xx}u(x,y,t) + \partial_{yy}u(x,y,t)$. This term corresponds to the movement of bacteria. For the biological reasons mentioned above, it is assumed that the clusters of two bacteria have a faster diffusion than the isolated bacteria, i.e. $\theta_2 > \theta_1$.

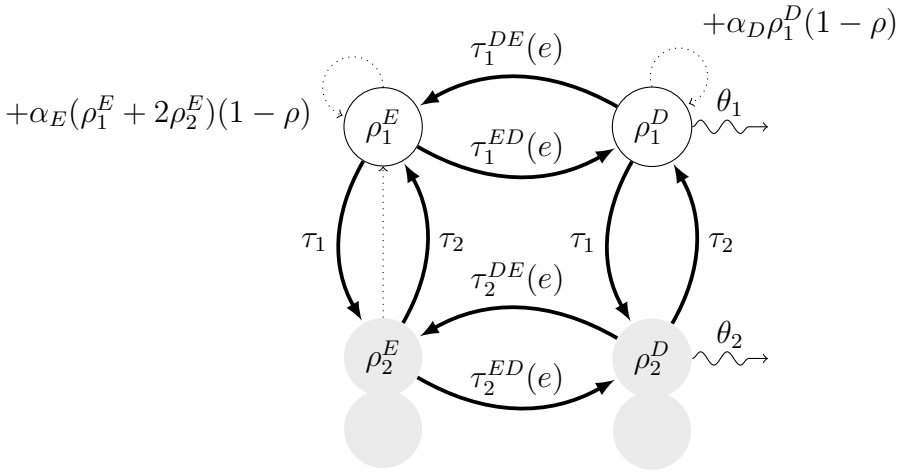

Figure 1: Schematic representation of the model (7)-(11)

We assume that the rates of transitions between the "diffusion" and the "eating" state are linearly dependent on the density of the prey e, i.e. τ_i^{DE} and τ_i^{ED} are given by

$$\tau_i^{DE}(e) = \tau_i^{DE} e, \quad \text{and} \quad \tau_i^{ED}(e) = \tau_i^{ED}(e_{\max} - e), \tag{12}$$

with $e_{\max}$ the maximum in space of $e(x, y, t = 0)$. As the density of the prey e decreases over time, $e_{\max}$ corresponds to the maximum of e in both time and space.

We perform a numerical analysis of this model. Simulations for different parameters show that the model exhibits similarities with the biological experiments of predation by the *Myxococcus xanthus* bacterium. We notice that, as expected, the sociability and the strong diffusion of the clusters play an important role in the speed of predation.

3 Discrete size model

3.1 Some properties of the mathematical model (1),(2)

We consider the equivalent nondimensional system given by

$$\partial_\tau \rho_1 = \partial_{\chi\chi}\rho_1 - k_1\rho_1^2 + 2k_2\rho_2 + \rho_1(1-\rho), \tag{13}$$

$$\partial_\tau \rho_2 = \theta\partial_{\chi\chi}\rho_2 + \frac{1}{2}k_1\rho_1^2 - k_2\rho_2, \tag{14}$$

where $\rho_i(\chi,\tau) = p_i(x,t)/\kappa$ for $i \in \{1,2\}$, $\chi = \sqrt{\alpha/\theta_1}x$, $\tau = \alpha t$, $\theta = \theta_2/\theta_1$, $k_1 = K\tau_1/\alpha$ and $k_2 = \tau_2/\alpha$ are the only three free parameters.

This model has a unique spatially homogeneous positive equilibrium point $\rho^\star = (\rho_1^\star, \rho_2^\star)$, given by

$$\rho_1^\star = 1 - 2\rho_2^\star, \quad \text{and} \quad \rho_2^\star = \frac{2k_1 + k_2 - \sqrt{k_2(4k_1+k_2)}}{4k_1},$$

with $\rho_1^\star + 2\rho_2^\star = 1$.

The point $(0,0)$ is another equilibrium point of the system (13)-(14). Linearising around these equilibrium points, we obtain the following Jacobian matrices

$$J(0,0) = \begin{pmatrix} 1 & 2k_2 \\ 0 & -k_2 \end{pmatrix}, \quad \text{and,} \quad J(\rho_1^\star, \rho_2^\star) = \begin{pmatrix} -2k_1\rho_1^\star - \rho_1^\star & 2k_2 - 2\rho_1^\star \\ k_1\rho_1^\star & -k_2 \end{pmatrix}.$$

The point $(0,0)$ is unstable while the point $\rho^\star$ is stable, therefore we are in a monostable case.

Asymptotics in fast fragmentation-coagulation regime.

In order to simplify the theoretical study of the system (13)-(14), we consider the limit where both rates k_1 and k_2 tend towards infinity at the same speed (in the sense that $k_1/k_2 < +\infty$ and $k_2/k_1 < +\infty$). This means that both cluster fragmentation and the coagulation of isolated bacteria occur at the same time scale, which is much faster than the growth and diffusion time scale. Equation (14) can be written

$$\partial_t \rho_2 - \theta\Delta\rho_2 = k_1\left(\frac{1}{2}\rho_1^2 - \frac{k_2}{k_1}\rho_2\right). \tag{15}$$

Since $k_1 \to +\infty$, we must have $\frac{1}{2}\rho_1^2 - \frac{k_2}{k_1}\rho_2 = 0$ in the RHS of Eq. (15). Then, recalling that $\rho = \rho_1 + 2\rho_2$ we obtain

$$\rho_1 = f(\rho) := \frac{-1 + \sqrt{1 + 4\frac{k_1}{k_2}\rho}}{2\frac{k_1}{k_2}}.$$

Therefore, since $2\rho_2 = \frac{k_1}{k_2}\rho_1^2 = \frac{k_1}{k_2}f(\rho)^2$, adding equations (13) and (14) yields

$$\partial_t \rho - \Delta\phi(\rho) = F(\rho), \tag{16}$$

with $\phi(\rho) := f(\rho) + \theta\frac{k_1}{k_2}f(\rho)^2$ and $F(\rho) := f(\rho)(1-\rho)$. Note that now $F(p) = 0$ if and only if $p = 0$ or $p = 1$ which are the only spatially homogeneous states. Differentiating twice the functions ϕ and F leads to

$$\phi''(x) = \frac{2k_1\,(\theta-1)}{(4k_1x+k_2)\sqrt{1+4\frac{k_1}{k_2}x}} \quad \text{and} \quad F''(x) = -2\frac{3k_1x+k_1+k_2}{(4k_1x+k_2)\sqrt{1+4\frac{k_1}{k_2}x}}.$$

Thereby, F is concave, positive and verifies $F(0) = F(1) = 0$. Moreover, we have that ϕ is convex if $\theta > 1$.

For the equation $\partial_t\rho - \theta\Delta\rho = F(\rho)$ with F concave, the minimal speed front is given by $c^* = 2\sqrt{\theta F'(0)}$ (see for instance [10]). On the other hand, the nonlinear diffusion term of Eq. (16) does not allow to directly apply this theory. Instead, we approach numerically the minimal speed employing a shooting method [22]. The method is based on the analysis of the phase plane $(\rho, (\phi(\rho))')$. We start by looking for solutions of the form

$$\rho(x,t) = p(x-ct), \quad (t,x) \in \mathbb{R}^2,$$

with c the unknown front speed that we want to determine. We are interested in solutions connecting the equilibrium state $p = 1$ (in $-\infty$) with the equilibrium state $p = 0$ (in $+\infty$). Then, from (16), we obtain

$$-cp' - (\phi(p))'' = F(p), \tag{17}$$

and if we set $q = (\phi(p))'$ we obtain the following system

$$\begin{cases} p' = \dfrac{1}{\phi'(p)}q, \\ q' = \dfrac{-c}{\phi'(p)}q - F(p), \\ \lim\limits_{\xi\to-\infty} p(\xi) = 1, \quad \lim\limits_{\xi\to+\infty} p(\xi) = 0. \end{cases}$$

So the problem is to find the wave speed $c \in \mathbb{R}$ and the $\mathcal{C}^2$ wave profile $p : \mathbb{R} \longrightarrow [0,1]$ that solves the previous system. For this, we perform a shooting method. We choose a certain value of c, small enough, and simulate the associated heteroclinic orbit solution p. If, at any point, p becomes negative, we reject the value of c and try a larger one, until obtaining an admissible profile. We will compare this speed with the one obtained by numerical simulations of the population dynamics. The method used and the results are given in the next paragraph and Figure 2, which is discussed further below.

3.2 Numerical simulations

We simulate Eq. (13)-(14) using a splitting method with a semi-implicit finite difference scheme. That is, we split the diffusion and reaction terms into two separate steps. For the first one, we use an implicit numerical scheme, and for the latter, we use the Runge-Kutta 4 explicit scheme.

Using this method, we numerically approximate solutions of (13)-(14) for different values of the cluster's relative diffusion coefficient $\theta > 1$ and for equal fragmentation and coagulation rates $k = k_1 = k_2 = k$. We vary both k and θ to study whether the total population density ρ behaves as a wave of the form $\rho(x,t) = u(x - ct)$ with $u(\xi) \sim \exp(-\lambda\xi)$. This exponential decay is observed in the Fisher-KPP equation and is expected from the study of the heterocline in the phase plane. The coefficient λ is the rate of exponential decay towards the stable state 0 and gives the form of the front. When we observe numerically that the density p indeed admits travelling wave solutions, we extract the values of c and λ from the simulated solutions of (13)-(14). The methods used are explained below.

Firstly, to obtain the wavespeed we compute at each time-step, $n\Delta t$, the estimator $\hat{c}_n$ defined by

$$\hat{c}_n := \sum_{j=1}^{J} \frac{\rho^n(x_j) - \rho^{n-1}(x_j)}{\Delta t} \Delta x, \tag{18}$$

where $\{x_j = j\Delta x\}_{j\in\{0,\dots,J\}}$ is the space grid and ρ^n is an approximation of $\rho(j\Delta x, n\Delta t)$. As $\Delta x, \Delta t \to 0$, $\hat{c}_n$ is consistent with the wavespeed. Indeed, if we suppose that we have wave solutions which are of the form $\rho(t,x) = u(x - ct)$, with $u(\xi) \to 1$ as $\xi \to -\infty$, and $u(\xi) \to 0$ as $\xi \to +\infty$, then $\partial_t \rho = -c\partial_x \rho$. Integration of this equation with respect to x gives

$$c = \int_{-\infty}^{+\infty} \partial_t \rho(t,x) dx. \tag{19}$$

Equation (18) is then a finite difference discretization of the time derivative and the spatial integral in the latter expression.

Secondly, the value λ of the exponential decay constant is computed by fitting an exponential curve to the wavefront, using a least squares estimator.

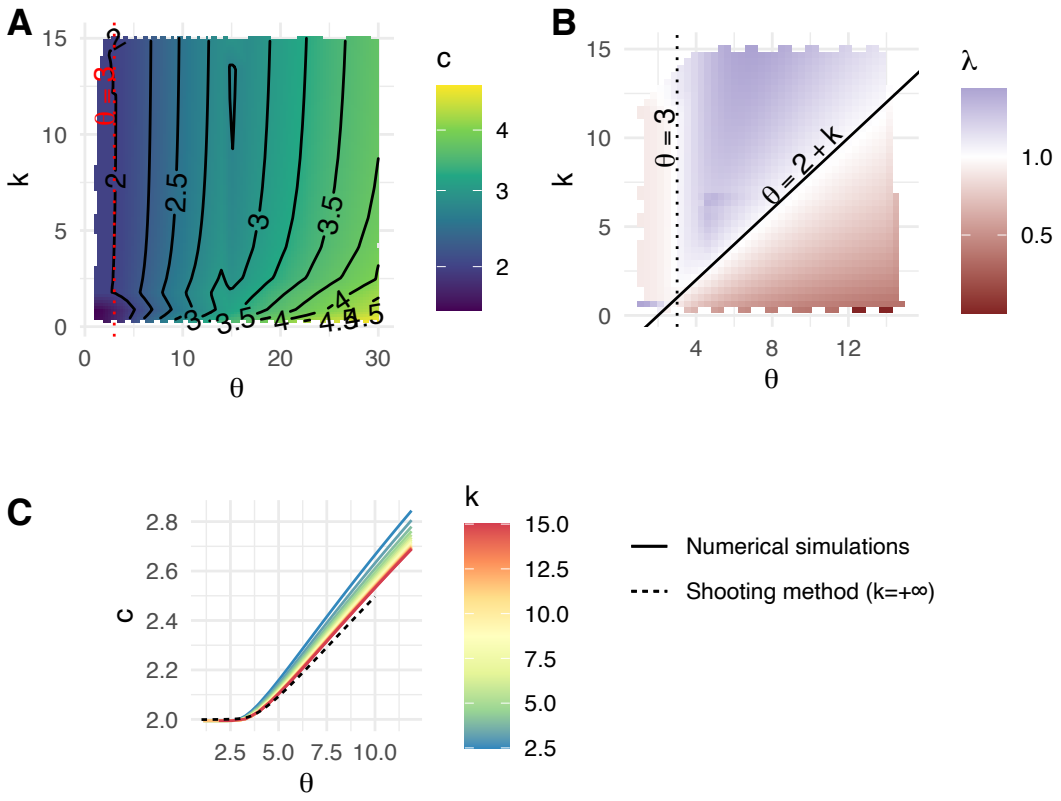

Figure 2: Numerical results of the nondimensional system of Eq. (13)-(14) for different values of the cluster's relative diffusion coefficient $\theta > 1$ and for equal fragmentation and coagulation rates $k = k_1 = k_2$. **A.** Wavefront propagation speed c as a function of θ and k. Contour levels are also indicated along the coloured heatmap. The speed is obtained using (18). The critical value of $c = 2$ is reached near the ordinate $\theta = 3$, highlighted in red. **B.** Exponential decay rate λ of the total population wavefront. The line $\theta = 2 + k$ corresponds to the regime change expected by the heuristic (Appendix A). **C.** Value of the wavefront speed c as a function of the clusters' diffusion coefficient θ, for various values of k (solid line). The value predicted by the shooting method described in Section 3.1 in the limit $k \to +\infty$ is also presented (dotted line).

Fig. 2 presents the results of c (panels A and C) and λ (panel B) extracted for $\theta \in [0, 30]$ and $k_1 = k_2 = k \in [0, 15]$. We recall that in the Fisher-KPP case, we have $c = 2$ and $\lambda = 1$. In particular, these values correspond to the regime where the cluster structure does not affect the propagation speed of the population. Fig. 2-A and 2-C shows the existence of a critical diffusion coefficient θ^* near the value $\theta = 3$ such that for all $\theta < \theta^*$ the wave speed corresponds to the Fisher-KPP speed, and, for all $\theta > \theta^*$, the speed is strictly larger than the Fisher-KPP speed. In the latter case, the speed of propagation is determined by the whole front, including the clusters of bacteria, which therefore contribute to the overall acceleration. To summarise, if the diffusion coefficient of the clusters is sufficiently larger than the diffusion coefficient of isolated bacteria (around 3 times larger), the whole population advances faster than in the Fisher-KPP case. Moreover, the value of this critical θ^* appears to be a constant for all $k > 0$, so this regime switch seems to be independent of the fragmentation-coagulation rate.

The analysis of the exponential decay of the front λ can shed light on the regime switching in speed. Fig. 2-B shows that the critical Fisher-KPP value of $\lambda = 1$ is reached in our simulations around two lines: first, around the constant $\theta = 3$, which corresponds to the observed threshold for the speed regimes; and second, around the line $\theta = 2 + k$. In particular, some heuristic calculations make it possible to explain formally this threshold (see Appendix A). However, it is observed that this line is not associated with a change of regime in the speed.

Finally, in Fig.2-C we can see the value of c approximated by the shooting method in the asymptotic $k \to +\infty$. These results, obtained trough a completely different numerical approach, confirm the independence of the threshold θ^* with respect to k and also help validate the results obtained from our numerical scheme.

4 Continuous cluster-size model

We make the following assumptions about the functions of the model (3)-(6)

$$\gamma(z', z) = \gamma z' z . \mathbf{1}_{z+z' \leq z_{\max}}, \quad \beta(z) = \beta z, \quad v(z, m) = \alpha z(1 - m/\kappa), \quad k(z', z) = \frac{1}{z'} \mathbf{1}_{z' > z}, \tag{20}$$

for $z \in [0, z_{\max}]$, with $\gamma > 0$ a constant coagulation rate by squared unit of size, $\beta > 0$ a constant fragmentation rate by unit of size, $\kappa > 0$ a carrying capacity with respect to the sum of the individual sizes of the population, and $\alpha > 0$ some constant growth rate by unit of size, and m is the total mass of the system as defined by Eq. (6). We assume that the function v is increasing to model the fact that the larger a cluster is, the higher the probability that one of its bacteria divides. In particular, when $m \approx 0$, the function v becomes linear, and each bacterium in a cluster has the same probability of dividing.

To begin with, we assume that the diffusion coefficient is defined by

$$\theta(z) = \theta_1, \qquad \text{for all } \ z \in [0, z_{\max}] \ . \tag{21}$$

Under the assumptions (20) and (21), we have the following equation for the moment of order 1,

$$\partial_t m = \theta_1 \partial_{xx} m + m\alpha(1 - m/\kappa). \tag{22}$$

Note that Eq. (22) corresponds to a Fisher-KPP equation, which admits traveling wave type solutions. Searching for a travelling wave solution for the model (3)-(6), we define the variable $\xi(t, x, z) = x - c(z)t$, where $c(z)$ is a function of z corresponding to the unknown invasion speed. We denote p the wave profile given by

$$\rho(t, x, z) = p(\xi(z), z), \tag{23}$$

with the following limits

$$p(-\infty, z) = f(z), \qquad p(+\infty, z) = \tilde{0}(z), \tag{24}$$

where $\tilde{0}$ corresponds to the null function and $f(z)$ to a stationary stable solution of the following system

$$\partial_t q(t, z) = -\partial_z \left[\alpha z(1 - M(t)/\kappa)\mathbf{1}_{z<z_{\max}}(z)q(t, z)\right] + \mathcal{F}[q](t, z) + \mathcal{G}[q](t, z), \quad \forall z \in (0, z_{\max}), \tag{25}$$

with

$$M(t) = \int_0^{z_{\max}} z' q(t, z') \, \mathrm{d}z'.$$

Moreover, we have $\lim_{t\to+\infty} M(t) \to \kappa$. Under the assumption $M \equiv \kappa$, equation (25) simplifies to the following coagulation-fragmentation equation.

$$\partial_t q(t,z) = \mathcal{F}[q](t,z) + \mathcal{G}[q](t,z). \tag{26}$$

In the article [23], under the assumption $z_{\max} = +\infty$, the authors derive the existence of the equilibrium profile for different assumptions than those in (20) regarding the functions β and γ. Nevertheless, as specified in Remark 5.2 of this article and in the article [24], it is possible to extend this result to our assumptions to obtain the profile of the stationary solution $f(z)$.

According to our numerical simulations, the equilibrium profile in the wake of the invasion front corresponds well to the stationary numerical solution of equation (26). For numerical simulations, we extended the method presented in Section 3.2.

In figure 3-A, we observe an example of a traveling wave type solution for the model (3)-(6). The initial data was chosen to be $\rho(x,z,0) = \tilde{f}(z)\mathbf{1}_{x\leq 30}$, where $\tilde{f}(z)$ is the numerical solution of the equation (25). Between times $t = 30$ and $t = 50$, the state $\tilde{f}(z)$ spatially invades the null state. According to our numerical simulations, for these parameter values, the speed of the traveling wave solutions of the equation (23) appears to be independent of z and is similar to the speed of the traveling waves of the moment of order 1 given by the equation (22). Traveling waves for the term m are illustrated in panel B of Figure 3. The colorimetry represents the progression of time, blue for $t = 0$ and red for $t = 80$. For this initial data, it is known that the selected speed of the traveling wave for m corresponds to the critical wave speed, *i.e.* $2\sqrt{\alpha\theta}$. In theory, if the system (3)-(6) admits solutions of traveling waves, the moments have them too. Moreover, the speed of the traveling waves of the moments is necessarily less than or equal to the speed of the traveling wave of the model (3)-(6).

Now, for the biological reasons mentioned above, we assume that θ is an increasing function of z. For numerical reasons, we define θ as

$$\theta(z) = \begin{cases} \theta_1\ , & \text{si } z \leq s, \\ \theta_2\ , & \text{si } z > s, \end{cases} \tag{27}$$

with θ_1, θ_2 two positive constant such that $\theta_2 > \theta_1$ and s a positive constant.

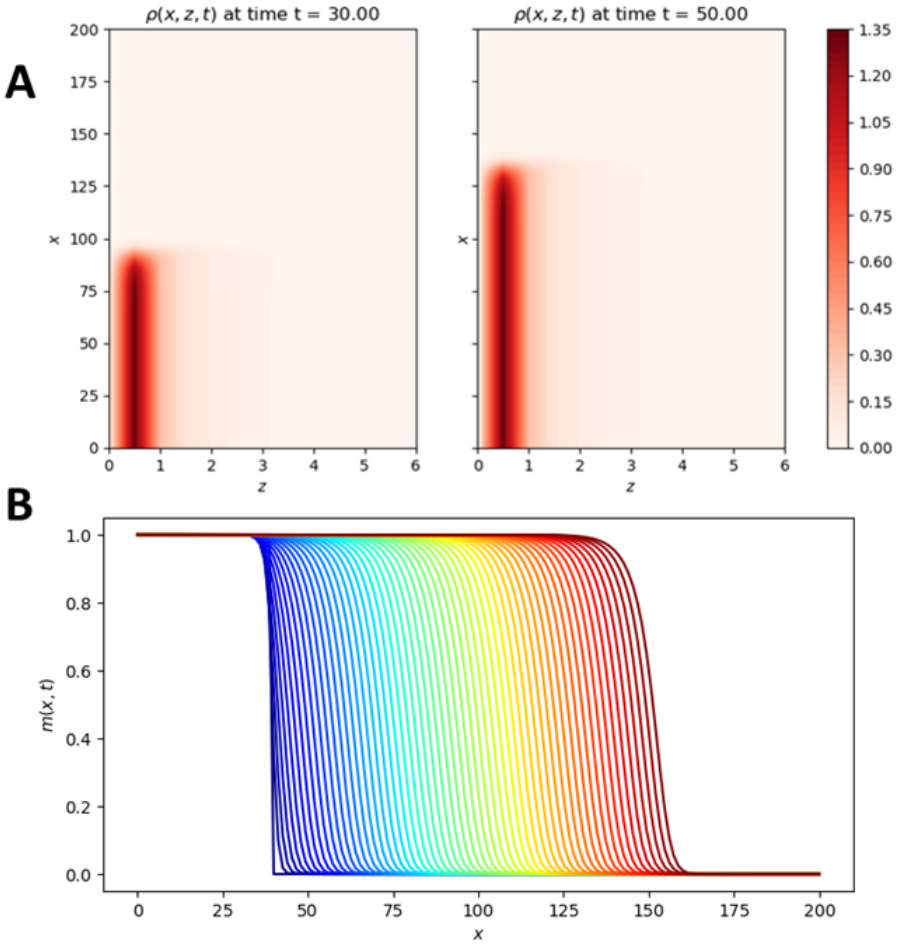

Figure 3: **A.** Example of a traveling wave for the model (3)-(6) under the assumptions (20) and (21). The state $f(z)$ spatially invades the state $\tilde{0}(z)$ for all z. Concerning the initial data, we assume that, at time $t = 0$, the density is given by $\rho(x, z, 0) = f(z)\mathbf{1}_{x \leq x_0}$ with some positive constant x_0. The parameter values are $\theta_1 = 1$, $\alpha = 1$, $\beta = 1$, $\gamma = 1$, $\kappa = 1$. **B.** Representation over time of the numerical solution $m(x, t)$. The color represents the time, blue $t = 0$ to red $t = T_{\text{end}}$ and the colorimetry is linear. The initial data and parameter values are the same as above.

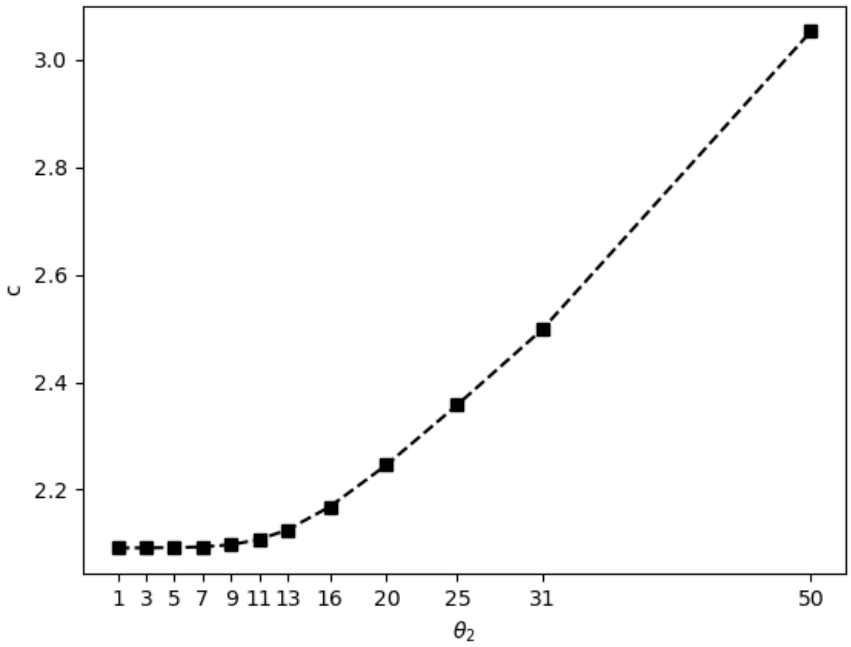

Figure 4: Speed of the traveling wave of the equation (22), obtained by numerical simulations, for different θ_2, under assumption (27). Similarly to the discrete model, there is a threshold $\tilde{\theta}_2$ such that for all $\theta_2 \leq \tilde{\theta}_2$ the speed of the wave is $c_{\text{KPP}} = 2\sqrt{\alpha\theta_1} = 2$, and for $\theta_2 > \tilde{\theta}_2$, the speed becomes strictly higher than the speed c_{KPP}. The parameter values are similar to those in Figure 3.

The figure 4 corresponds to the evolution of the numerical speed of the traveling wave of the moment of order 1 as a function of θ_2, for the model (3)-(6) with θ defined by (27). Once again, we observe, the existence of a threshold $\tilde{\theta}_2$. Indeed, for $\theta_2 \leq \tilde{\theta}_2$, we notice that the speed of the traveling wave seems to be very close to the speed $c_{\text{KPP}} = 2\sqrt{\theta_1\alpha}$ and becomes strictly larger for $\theta_2 > \tilde{\theta}_2$. For θ_2 sufficiently large (larger than the interval θ in Figure 4), we notice that the growth is of order $\sqrt{\theta_2}$, similar to the discrete model (1)-(2).

5 Resource-predator model

Figure 5 corresponds to the numerical simulation of the system (7)-(11) which takes into account two types of bacteria. The first type ρ_i^E is immobile and can consume its prey, while the second ρ_i^D diffuses. The density of the prey, for example *E. coli*, is shown in red. The green color corresponds to the density of diffusing bacteria $\rho_1^D + 2\rho_1^D$, and in blue the bacteria that consume the prey, $\rho_1^E + 2\rho_1^E$. The initial data, represented in the figure 5 (top panel) are chosen to be as close as possible to the biological experiments. At first the bacteria are in the "diffusion" state, looking for prey. Some of the diffusing bacteria will, on contact with the prey, change state to become bacteria that consume the prey. This behavior tends to reduce the spread of predation in areas with high prey density. For example, the propagation of predatory bacteria is faster in the middle of *E. coli* than on these edges with a higher initial density (See Figure 5 lower left panel). Gradually, the prey will be consumed and will disappear.

To understand the importance of sociability in predator propagation, we define a model similar to the system (7)-(11) for which isolated bacteria cannot regroup to form a cluster. The model is defined by

$$\begin{cases} \partial_t\ \rho_1^D = \theta_1 \Delta \rho_1^D + \alpha_D \rho_1^D (1-\rho) - \tau_1^{DE}(e)\rho_1^D + \tau_1^{ED}(e)\rho_1^E, \\ \partial_t\ \rho_1^E = \tau_1^{DE}(e)\rho_1^D - \tau_1^{ED}(e)\rho_1^E + \alpha_E \rho_1^E (1-\rho), \\ \partial_t\ e = -\delta_1 \rho_1^E, \\ \rho = \rho_1^D + \rho_1^E. \end{cases} \tag{28}$$

In the figure 6 we observe the importance of sociability on the speed of predation. The left part corresponds to the numerical simulation of the model (28) at time $t = 0$ and at time $t = 8$ and on the right it corresponds to the numerical simulation of the system (7)-(11) at the same times. For both simulations we take similar initial data and parameters shared by both models have the same values. Under these assumptions, we observe in Figure 6 (bottom panel) that for the (7)-(11) model, the prey, shown in red, is consumed faster.

The speed of predation is strongly correlated with the value of the parameter θ_2. Contrary to the previous model, the lesser advantage given to clusters has an effect on the predation speed. The figure 7 corresponds to two numerical simulations of the system

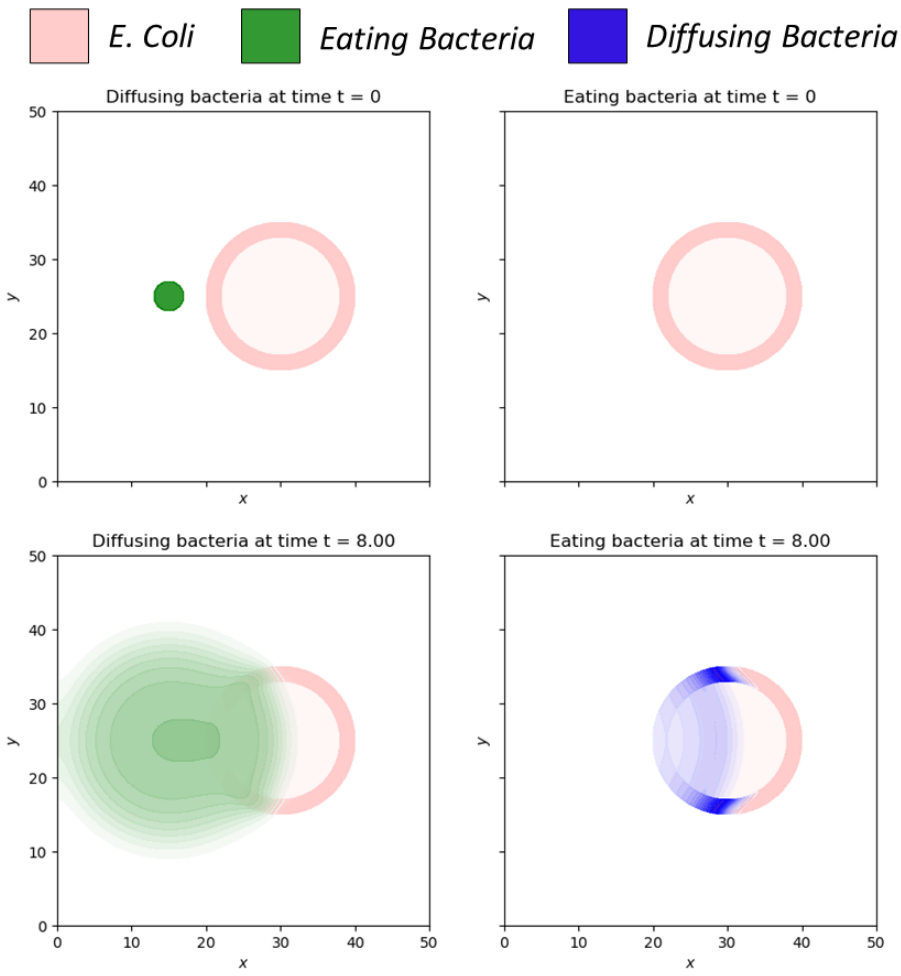

Figure 5: Numerical simulations of the model (7)-(11), under the assumption (12). The density of bacteria that diffuse, $\rho_1^D + 2\rho_2^D$, is represented in green and the density of bacteria that consume the prey, $\rho_1^E + 2\rho_2^E$, is represented in blue. The prey density, e, is represented in red. The initial data are shown in the top panel, they are chosen to be as close as possible to the biological experiments. The initial distribution of predatory bacteria is assumed to be homogeneous on a circle, while the initial distribution of prey is assumed to be arranged on a circle with a higher density at the edges. At time $t = 0$, there are no predatory bacteria in the "eating" state. The bottom panel represents the densities at time, $t = 8$, where predatory bacteria have spread and reached the prey, which then began to consume the prey. The parameter values for this numerical simulation are $\theta_1 = 1$, $\theta_2 = 2$, $\alpha_D = 1$, $\alpha_E = 3$, $\tau_1 = 2$, $\tau_2 = 1$, $\tau_1^{DE} = \tau_2^{DE} = 1$, $\tau_1^{ED} = \tau_2^{ED} = 1$, $\delta_1 = \delta_2 = 2$.

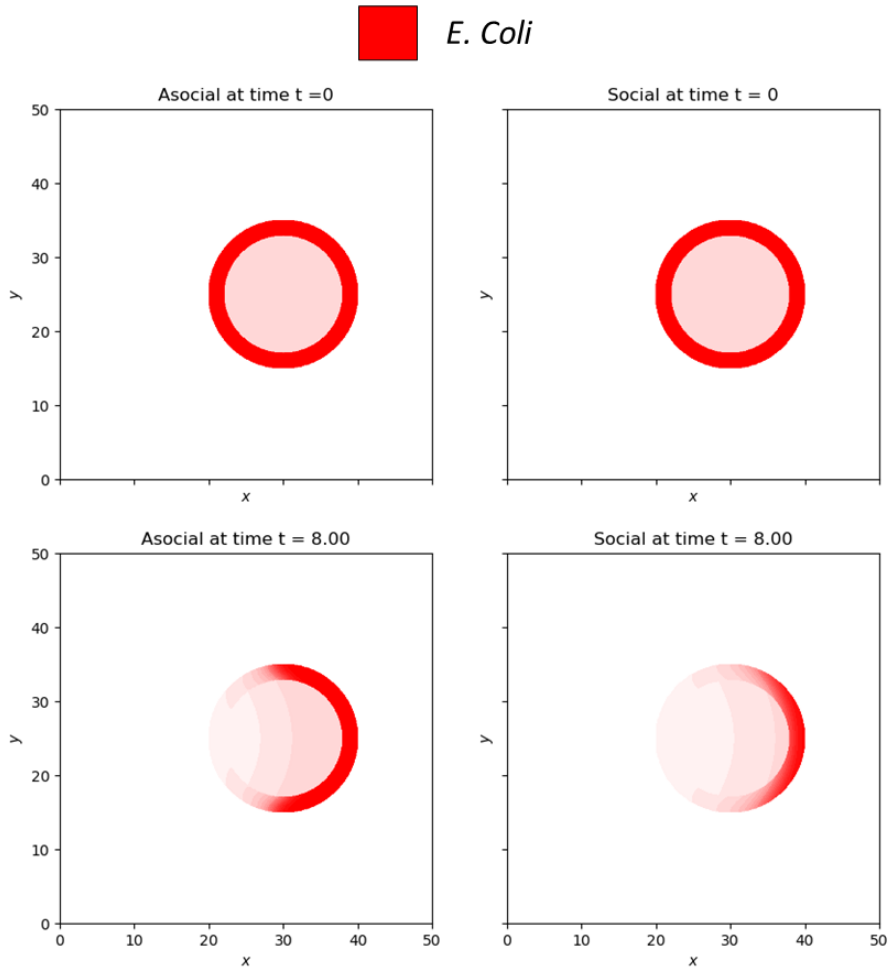

Figure 6: The distribution of *E. coli* at time $t = 0$ (top) and $t = 8$ (bottom) is represented in red, for the model (28) (left) and for the model (7)-(11) (right). For both simulations, we assume the linear transition hypothesis (12). We assume that there are no advantages/disadvantages other than diffusion, therefore $\delta_2 = \delta_1$, $\tau_2^{ED} = \tau_1^{ED}$ and $\tau_2^{DE} = \tau_1^{DE}$. Under this assumption, predation is faster for the model (7)-(11) than for the model (28). The values of the parameters are the same as in figure 5.

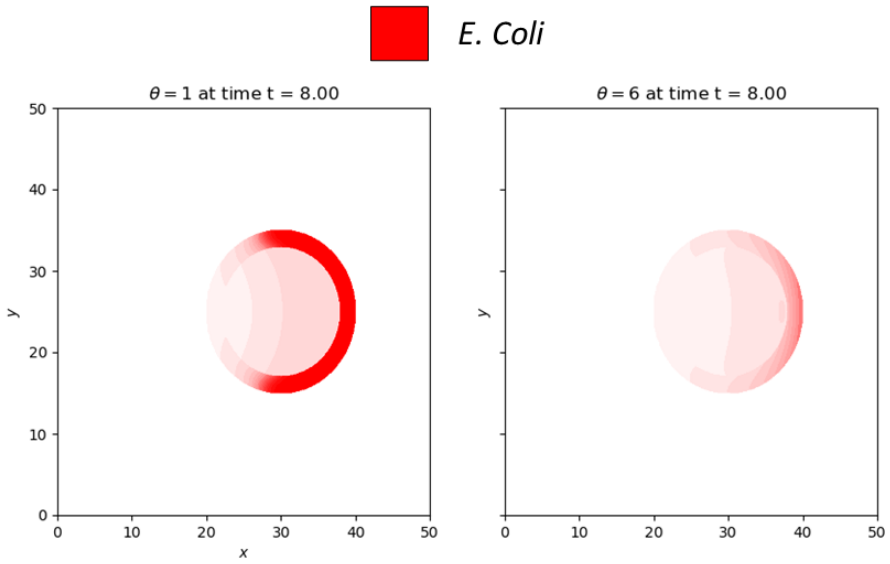

Figure 7: Numerical simulations of the model (7)-(11) with different diffusion coefficients. The distribution of *E. coli* is represented in red at time $t = 8$ with the same initial data. The coefficient θ is defined as the ratio of θ_2 and θ_1, *i.e.* $\theta := \theta_2/\theta_1$ and corresponds to the advantage/disadvantage of cluster diffusion. For the simulation on the left, we assume that $\theta = 1$ and for the simulation on the right we assume that $\theta = 6$. The values of the other parameters are the same for both simulations and are those in figure 5.

(7)-(11) at time $t = 8$ for two different coefficients θ_2. The other parameter values and the initial data are similar. The prey density, represented in red, is much lower for a larger θ_2 coefficient. We observe that the speed of predation is an increasing function of $\theta := \theta_2/\theta_1$, for $\theta > 1$.

6 Conclusions and perspectives

We studied the effect of social behaviour on the motility of *Myxococcus xanthus* populations. Previous *in vitro* experiments have shown that the capacity to form clusters of bacteria that move collectively begets an enhanced predation efficiency. Our numerical experiments shed some light on this phenomenon. We have first considered a minimal model in which isolated bacteria are able to form clusters of two bacteria that diffuse collectively. The simulations suggest that when the clusters diffuse at least 3 times faster

than the isolated individuals, the speed of propagation of the whole population is larger than the critical Fisher-KPP speed. Otherwise, if clusters do not diffuse fast enough, the speed of the population is limited by the propagation speed of isolated individuals. The threshold separating these two regimes seems to be unique and independent of the rates of fragmentation and coagulation. In particular, using a shooting method, the same regime separation was found numerically in the asymptotic case of infinitely fast fragmentation and coagulation.

We also considered two extensions. First, we studied a continuous cluster-size model expressed as an integro-differential equation with fragmentation and coagulation operators. Under biologically relevant parameterizations for these operators, we show that the total sum of cluster sizes (first order moment) of the structured population exhibit travelling waves whose speed is also characterised by a threshold in the diffusion coefficient, below which the speed coincides with Fisher-KPP critical speed. This result seems to extend the regime separation observed in the discrete case to a more general class of population dynamics. In this case, as the population wavefront advances, the cluster structure of the rear of the wave is distributed according to the steady-state distribution of cluster sizes, and the travelling wave connects the steady-state to the null function.

Finally, we considered an extended model in which both isolated and clustered bacteria have the ability to switch towards an *eating* state when they encounter a positive density of prey. However, they become immobile in this state. With the purpose of observing the effect of clusters in the predatory efficiency, we compared the propagation fronts obtained in presence and absence of clustering. Numerical simulations indicate that the prey is consumed faster when bacteria are allowed to cluster. In this case, the speed of predation is an increasing function of the ratio of the diffusion coefficients of clusters and isolated bacteria.

Regime separation in the discrete case, particularly in the fast fragmentation-coagulation asymptotic, can motivate some theoretical investigations that are not explored here. For example, approaches relying in the variational characterisation of the wave speed can be adapted to obtain bounds on the diffusion threshold θ^*. The numerical simulations can also be extended to include some more realistic cases, taking into account the complex

cluster structure of swarms and scouts.

Acknowledgements

This project has received funding from the European Research Council (ERC) under the European Union's Horizon 2020 research and innovation programme (grant agreement No 865711). M.E. was funded by the ANR via the project PLUME under grant agreement ANR-21-CE13-0040. I.M. was supported by the Chair Modélisation Mathématique et Biodiversité of Veolia Environnement - École polytechnique - Museum National d'Histoire Naturelle - Fondation X and was funded by the European Union (ERC, SINGER, 101054787). The authors would also like to thank the organisers of CEMRACS 2022 (Emmanuel Franck, Hélène Hivert, Guillaume Latu, Hélène Leman, Bertrand Maury, Michel Mehrenberger, Laurent Navoret) for the stimulating research environment in the context of which this work was developed. We acknowledge particularly Hélène Hivert for our fruitful discussions concerning the numerical schemes. We would also like to thank Florence Hubert for her valuable insights and discussions related to this project.

Appendix A Heuristics on the $\theta = 2+k$ threshold line

We give some explanations on the critical threshold $\theta = 2+k$ observed in Fig. 2-B at which $\lambda = 1$. To that extent, we assume the existence of a wavefront solution $\rho(t,x) = \rho(x-ct)$ with unknown speed c. Let $\xi = x - ct$. PDE system (13)-(14) reduces to the following system of second-order ODE on the variable z:

$$\begin{cases} -c\partial_\xi \rho_1 = \partial_{\xi\xi}\rho_1 - k_1\rho_1^2 + 2k_2\rho_2 + \rho_1\left(1-\rho\right), \\ -c\partial_\xi \rho_2 = \theta\partial_{\xi\xi}\rho_2 + \frac{1}{2}k_1\rho_1^2 - k_2\rho_2, \\ \rho = \rho_1 + 2\rho_2. \end{cases}$$

Now, let's suppose that in the forefront of the population the number of isolated individuals and clusters is such that we are under the following hypothesis

$$(H_0): \qquad \rho_1^2 \ll \rho_2 \ll \rho_1.$$

Under (H_0), the first ODE becomes

$$-c\rho_1 = \partial_{\xi\xi}\rho_1 - \rho_1.$$

This is equivalent to the linearisation of Fisher-KPP Equation, for which the critical speed is $c = 2$. Moreover, the solution profile is of the form $\rho_1(z) = C_1 \exp(-\lambda\xi)$, with $\lambda = 1$. Now, let's come back to the second ODE and replace ρ_1. We get

$$-c\partial_\xi\rho_2 - \theta\partial_{\xi\xi}\rho_2 + k_2\rho_2 = \frac{k_1}{2}C_1^2 e^{-2\lambda\xi.}$$

We solve this equation finding a solution of the form

$$\rho_2(\xi) = Ae^{-\mu\xi} + Be^{-2\lambda\xi}.$$

In particular, for the particular solution, the constant B is such that

$$\left(2\lambda c - 4\theta\lambda^2 + k_2\right) B = \frac{k_1}{2}C_1^2.$$

Thus, at the critical value $\lambda = 1$ we obtain

$$\left(2c - 4\theta + k_2\right) B = \frac{k_1}{2}C_1^2,$$

which for $2c - 4\theta + k_2 \neq 0$ begets

$$B = \frac{C_1^2 k_1}{2\left(2c - 4\theta + k_2\right)}.$$

On the other hand, for the constant μ, we have:

$$c\mu - \theta\mu^2 + k_2 = 0.$$

Thus, for $\Delta = c^2 + 4\theta k_2 > 0$, we obtain the solutions:

$$\mu_\pm = \frac{-c \pm \sqrt{c^2 + 4\theta k_2}}{-2\theta} = \frac{c \mp \sqrt{c^2 + 4\theta k_2}}{2\theta}.$$

Since $\mu_+ < 0$, we consider only the solution with $\mu = \mu_-$. The critical transition should occur when H_0 is not verified anymore, and thus the nonlinear effects are not negligible. In particular, when we are just at the threshold level, we also have the critical Fisher-KPP values $\mu = 1$ and $c = 2$ which gives

$$\sqrt{1 + \theta k_2} = \theta - 1,$$

from which we derive the relation $\theta = 2 + k_2$. Therefore we should expect that, at fixed k_2, (H_0) is violated for all $\theta > 2 + k_2$.

References

[1] Swapnesh Panigrahi et al. "Misic, a general deep learning-based method for the high-throughput cell segmentation of complex bacterial communities". In: *Elife* 10 (2021), e65151.

[2] James A Shapiro. "Thinking about bacterial populations as multicellular organisms". In: *Annual review of microbiology* 52.1 (1998), pp. 81–104.

[3] Simon V Avery. "Microbial cell individuality and the underlying sources of heterogeneity". In: *Nature Reviews Microbiology* 4.8 (2006), pp. 577–587.

[4] Yong Zhang et al. "From individual cell motility to collective behaviors: insights from a prokaryote, Myxococcus xanthus". In: *FEMS microbiology reviews* 36.1 (2012), pp. 149–164.

[5] Sara Rombouts et al. "Multi-scale dynamic imaging reveals that cooperative motility behaviors promote efficient predation in bacteria". In: *Nature Communications* 14.1 (2023), p. 5588.

[6] Jonathan Hodgkin and Dale Kaiser. "Genetics of gliding motility in Myxococcus xanthus (Myxobacterales): two gene systems control movement". In: *Molecular and General Genetics MGG* 171.2 (1979), pp. 177–191.

[7] Sofiene Seef et al. "A Tad-like apparatus is required for contact-dependent prey killing in predatory social bacteria". In: *Elife* 10 (2021), e72409.

[8] Hélène Bloch et al. "A new modeling approach of myxococcus xanthus bacteria using polarity-based reversals". working paper or preprint. May 2023. URL: `https://hal.science/hal-04102694`.

[9] Ronald Aylmer Fisher. "The wave of advance of advantageous genes". In: *Annals of eugenics* 7.4 (1937), pp. 355–369.

[10] Andrei N Kolmogorov. "A study of the equation of diffusion with increase in the quantity of matter, and its application to a biological problem". In: *Moscow University Bulletin of Mathematics* 1 (1937), pp. 1–25.

[11] Hans F Weinberger, Mark A Lewis, and Bingtuan Li. "Anomalous spreading speeds of cooperative recursion systems". In: *Journal of mathematical biology* 55 (2007). Publisher: Springer, pp. 207–222.

[12] Jimmy Garnier et al. "Inside dynamics of pulled and pushed fronts". In: *Journal de mathématiques pures et appliquées* 98.4 (2012), pp. 428–449.

[13] Maxime Estavoyer and Thomas Lepoutre. "Travelling waves for a fast reaction limit of a discrete coagulation-fragmentation model with diffusion and proliferation". working paper or preprint. Mar. 2024. URL: `https://hal.science/hal-04516285`.

[14] A Ducrot and P Magal. "Travelling wave solutions for an infection-age structured model with diffusion". In: *Proceedings of the Royal Society of Edinburgh Section A: Mathematics* 139.3 (2009), pp. 459–482.

[15] Emeric Bouin and Vincent Calvez. "Travelling waves for the cane toads equation with bounded traits". In: *Nonlinearity* 27.9 (2014), p. 2233.

[16] Matthieu Alfaro, Jérôme Coville, and Gaël Raoul. "Travelling waves in a nonlocal reaction-diffusion equation as a model for a population structured by a space variable and a phenotypic trait". In: *Communications in Partial Differential Equations* 38.12 (2013), pp. 2126–2154.

[17] Quentin Griette. "Singular measure traveling waves in an epidemiological model with continuous phenotypes". In: *Transactions of the American Mathematical Society* 371.6 (2019), pp. 4411–4458.

[18] Ryan Keane and James Berleman. "The predatory life cycle of Myxococcus xanthus". In: *Microbiology* 162.1 (2016), pp. 1–11.

[19] Kristina L Hillesland, Gregory J Velicer, and Richard E Lenski. "Experimental evolution of a microbial predator's ability to find prey". In: *Proceedings of the Royal Society B: Biological Sciences* 276.1656 (2009), pp. 459–467.

[20] Mark J McBride and David R Zusman. "Behavioral analysis of single cells of Myxococcus xanthus in response to prey cells of Escherichia coli". In: *FEMS microbiology letters* 137.2-3 (1996), pp. 227–231.

[21] James E Berleman and John R Kirby. "Deciphering the hunting strategy of a bacterial wolfpack". In: *FEMS microbiology reviews* 33.5 (2009), pp. 942–957.

[22] Mike R Osborne. "On shooting methods for boundary value problems". In: *Journal of mathematical analysis and applications* 27.2 (1969), pp. 417–433.

[23] Pierre Degond, Jian-Guo Liu, and Robert L Pego. "Coagulation–fragmentation model for animal group-size statistics". In: *Journal of Nonlinear Science* 27 (2017), pp. 379–424.

[24] Philippe Laurençot. "Stationary solutions to coagulation-fragmentation equations". In: *Annales de l'Institut Henri Poincaré C, Analyse non linéaire*. Vol. 36. 7. Elsevier. 2019, pp. 1903–1939.